Analytical Methods

PAPER

View Article Online
View Journal | View Issue

Cite this: *Anal. Methods*, 2015, **7**, 2585

Highly sensitive aptasensor for oxytetracycline based on upconversion and magnetic nanoparticles

Congcong Fang, Shijia Wu, Nuo Duan, Shaoliang Dai and Zhouping Wang*

A novel sensitive aptasensor was developed for the quantification of oxytetracycline (OTC) in this study. Artificial aptamer-modified magnetic nanoparticles (aptamer-MNPs) were employed as capture probes, and complementary oligonucleotide-modified upconversion nanoparticles (cDNA-UCNPs) were used as signal probes. Then, the probes were hybridized to form poly-network structure MNPs-UCNPs signal probes. Finally, when the target was introduced, the aptamer combined with the priority target and the signal probe was replaced. The proposed method achieved a linear range between 0.05 and 100 ng mL^{-1}, and the limit of detection (LOD) was as low as 0.036 ng mL^{-1}, benefiting largely from labeling with UCNPs, aptamer affinity and magnetic separation. Then, we successfully applied the method to measure OTC in milk samples and validated it by a commercially available enzyme-linked immunosorbent assay (ELISA) method. The results demonstrated that the method possessed high sensitivity and good selectivity for the determination of OTC and is applicable to the determination of OTC in food samples.

Received 22nd December 2014
Accepted 25th January 2015

DOI: 10.1039/c4ay03035d

www.rsc.org/methods

1 Introduction

With a unique upconversion mechanism that enables the conversion of low-energy photons (near-infrared photons) into high-energy photons (visible to ultraviolet photons) *via* multi-photon processes, lanthanide-doped upconversion nanoparticles (UCNPs) have attracted enormous attention in recent years.[1–3] Upconversion nanoparticles possess immense advantages in biological applications over other types of fluorescent materials (*e.g.*, organic dyes, fluorescent proteins, gold nanoparticles, quantum dots, and luminescent transition metal complexes),[4] including low toxicity, large Stokes shifts, high quantum yields, high resistance to photobleaching, blinking, photochemical stability and the lack of both auto-luminescence and a light-scattering background, which consequently results in detection with high sensitivity and signal-to-noise ratio.[5–10] Moreover, magnetic nanoparticles (MNPs) with good biocompatibility and rapid separation from substrate solutions have been extensively applied in the field of biological detection.[11–13]

Tetracyclines (TCs) are broad-spectrum antibiotics that include oxytetracycline, which is likely the most widely used antibacterial in aquaculture.[14] The presence of tetracycline residues, especially oxytetracycline (OTC), from animal-derived foods poses a great risk to human health, such as allergic reactions, toxic effects and the development of resistance in microorganisms to antibiotics.[15,16] Therefore, researchers have made significant efforts to develop methods to identify and quantify OTC, such as HPLC-DAD and LC-MS/MS.[17,18] Although sensitive and accurate, these methods demand expensive equipment, tedious sample extraction procedures and technical skills.[19] Similarly, although having a wide range of application and low testing costs, immunochemical methods using antibodies usually lack specificity and sensitivity, due to high similarity in the structure of tetracycline derivatives. In addition, these methods are unstable because antibodies are sensitive to pH, temperature and other physicochemical factors in biological samples.[20,21] Therefore, there is still a demand to develop sensitive and specific methods to detect OTC.

Aptamers are DNA or RNA molecules which can adopt specific three-dimensional conformations to combine with target analytes. Compared with antibodies, aptamers are more stable, are easier to synthesize, can be modified in bulk and have many other advantages.[22,23] To the authors' knowledge, a series of aptasensors for OTC have been developed.[24–30] Though the reported electrochemical, colorimetric light scattering and microcantilever methods should be highly sensitive, they are of limited utility because of either high background signal or instability in biological samples, due to the inherent characteristics of the nanoparticles used, and can be difficult to utilize for on-site detection because of the tedious immobilization steps of the aptamers.[31] Therefore, it is desirable to overcome the above limitations and to search for a simple and sensitive aptamer-based detection method for OTC.

Here, we present an aptasensor for OTC based on upconversion and magnetic nanoparticles, possessing excellent

State Key Laboratory of Food Science and Technology, Synergetic Innovation Center of Food Safety and Nutrition, School of Food Science and Technology, Jiangnan University, Wuxi 214122, China. E-mail: wangzp@jiangnan.edu.cn; Fax: +86-510-85917023; Tel: +86-510-85917023

sensitivity and selectivity, lacking in interference from autoluminescence of other biomolecules. Artificial aptamer-modified magnetic nanoparticles (aptamer-MNPs) were employed as capture probes, and complementary DNA strand-modified upconversion nanoparticles (cDNA-UCNPs) were used as signal probes. Then the probes were hybridized to form poly-network structure MNPs-UCNPs signal probes. Finally, when the target was introduced, the aptamer combined with the priority target and the signal probe was replaced. Thus, a novel analytical method has been successfully applied to the detection of OTC, relying on labeling with UCNPs, aptamer selectivity and magnetic separation. In addition, the detection limit was as low as 0.036 ng mL^{-1}. To our knowledge, this is the first report to detect OTC using UCNPs and an aptamer. Furthermore, as UNCPs can be doped with lanthanide ions, such as Er^{3+}, Ho^{3+} and Tm^{3+}, this proposed method has great potential in the detection of structurally similar tetracycline derivatives based on multicolored UCNPs.

2 Experiments

2.1 Materials and chemicals

The rare earth chlorides and nitrates used in this work, including $YCl_3 \cdot 6H_2O$, $YbCl_3 \cdot 6H_2O$, $ErCl_3 \cdot 6H_2O$, $Y(NO_3)_3 \cdot 6H_2O$, $Yb(NO_3)_3 \cdot 5H_2O$, and $Er(NO_3)_3 \cdot 5H_2O$, were of 99.99% purity and were purchased from Aladdin Industrial Inc. (Shanghai, China). Oleic acid, octadecene (ODE), cyclohexane, 25% ammonia, 25% glutaraldehyde ($OHC(CH_2)_3CHO$), iron trichloride ($FeCl_3 \cdot 6H_2O$), tetraethyl orthosilicate (TEOS), 1,6-hexanediamine and ethanol were of analytical grade and were purchased from Sinopharm Chemical Reagent Co., Ltd. (Shanghai, China). IGEPAL CO-520 and 98% 3-aminopropyltrimethoxysilane (APTES) were purchased from Alfa Aesar (USA). OTC aptamer (reported by Javed H. Niazi *et al.*[25]) and its partially complementary strand were synthesized by Shanghai Sangon Biological Science & Technology Company (Shanghai, China). The sequence of the OTC aptamer was 5′-NH_2-GGAATTCGCTAGCACGTTGACGCTGGTGCCCGGTTGTGGTGCGAGTGTTGTGTGGATCCGAGCTCCACGTG-3′ (aptamer). The sequence of its partially complementary strand was 5′-NH_2-CGGATCCACACAACA-3′ (cDNA). Oxytetracycline (OTC), tetracycline (TET), and doxycycline (DOX) were purchased from Aladdin Reagent Co., Ltd. (Shanghai, China).

2.2 Apparatus

The size and morphology of nanoparticles were observed on a JEM-2100HR transmission electron microscope (TEM, JEOL Ltd., Japan), using an accelerating voltage of 200 kV. X-ray diffraction (XRD) measurements were performed using a D8 Advance instrument (Bruker AXS Ltd., Germany) with graphite-monochromated Cu-Kα radiation ($\lambda = 0.15406$ nm). The luminescence spectra of UCNPs were measured on an F-7000 luminescence spectrophotometer (Hitachi Co., Japan) attached to an external 980 nm laser (Beijing Hi-Tech Optoelectronic Co., China) instead of an internal excitation source. The maximum power of the laser was 1300 mW. FTIR spectra of amino-modified NPs were measured with a Nicolet Nexus 470 Fourier transform infrared spectrophotometer (Thermo Electron Co., USA) using the KBr method. Ultraviolet-visible (UV-vis) absorption spectra were recorded using a Shimadzu UV-2300 UV-vis spectrophotometer (Shimadzu, Japan) and the concentration of oligonucleotides was measured using a One Drop OD-1000 spectrophotometer (OneDrop Technologies, Inc., USA).

2.3 Synthesis and surface modification of rare-earth-doped $NaYF_4$:Yb, Er upconversion nanoparticles

$NaYF_4$:18% Yb, 2% Er UCNPs were synthesized by the method described by Zhengquan Li and Yong Zhang, with some modifications.[32] All the doping ratios of Ln^{3+} ions referred to molar ratios in our experiments. In brief, YCl_3, $YbCl_3$ and $ErCl_3$ were mixed with 6 mL oleic acid and 17 mL octadecene in a 50 mL flask, heated to 160 °C to form a homogeneous solution, and then cooled to room temperature. A 10 mL methanol solution containing NaOH and NH_4F was slowly added to the flask. The solution was stirred for 30 min and the temperature was raised to evaporate the methanol, then the solution was degassed at 100 °C for 10 min, before being heated to 300 °C and maintained for 1 h under an argon atmosphere. After the solution was cooled, nanocrystals were precipitated from the solution with ethanol and washed with ethanol–water (1 : 1 v/v) three times.

Surface modification of the $NaYF_4$:Yb, Er UCNPs was completed using a microemulsion method to coat silica onto the surface of the UCNPs.[33] Then 500 μL CO-520 and 10 mL cyclohexane containing $NaYF_4$ nanospheres were mixed and stirred for 10 min, then ammonia was added and the solution was sonicated for 20 min until a transparent emulsion was formed. TEOS and APTES were added to the solution, and the solution was stirred for two days at a speed of 600 rpm. Silica/$NaYF_4$ nanospheres were precipitated by adding acetone, and the nanospheres were washed with ethanol–water.

2.4 Preparation of amino-modified Fe_3O_4 magnetic nanoparticles (MNPs)

To prepare MNPs, a one-pot synthetic method was adopted.[34] For ~25 nm magnetic nanoparticles, a solution of 1,6-hexanediamine (6.5 g), anhydrous sodium acetate (2.0 g) and $FeCl_3 \cdot 6H_2O$ (1.0 g) as a ferric source in glycol (30 mL) was stirred vigorously to give a transparent solution. This solution was then transferred into a Teflon-lined autoclave and reacted at 198 °C for 6 h. The magnetic nanoparticles were then rinsed with water and ethanol (2 or 3 times), to effectively remove the solvent and unbound 1,6-hexanediamine, and then dried before characterization and application. During each rinsing step, the nanoparticles were separated from the supernatant using magnetic force.

2.5 Preparation of signal probes and capture probes

The procedure for the preparation of oligonucleotide-conjugated MNPs and UCNPs was adapted from the classical glutaraldehyde method.[35] 10 mg amino-modified nanoparticles was dispersed in 5 mL phosphate buffer solution (PBS) at pH 7.4 by

ultrasonication for 15 min, and then 0.2 mL 25% glutaraldehyde was added to the mixture. The mixture was shaken slowly on a shaking table at room temperature for 2 h. After incubation, the MNPs were separated by an external magnetic field and the UCNPs were separated by centrifugation. The nanoparticles were washed with phosphate buffer solution three times and dispersed in 5 mL PBS buffer solution.

Then an amino-modified aptamer was added to the glutaraldehyde-modified MNPs and amino-modified cDNA was added to the glutaraldehyde-modified UCNPs. The mixture was then incubated at 37 °C for another 2 h. After removal of the supernatant and washing, the resulting solution was resuspended in fresh STE buffer (10 mM Tris–HCl, pH 8.0, 50 mM NaCl, 1 mM EDTA) and stored at 4 °C.

2.6 Procedure for the detection of OTC

A total of 100 μL of aptamers-MNPs was hybridized in STE buffer with the optimized cDNA-UCNPs at 37 °C for 2 h to obtain UCNPs-MNPs signal probes. The UCNPs-MNPs probes were separated by a magnetic field and resuspended in PBS buffer. Then various concentrations of OTC standard were added to the mixture and further incubated at 37 °C for 2 h. The remaining UCNPs-MNPs were then separated and washed three times, and the luminescence intensity was measured with a 980 nm excitation laser.

2.7 Method comparison with ELISA analysis in food samples and recovery experiment

The accuracy of OTC detection in food samples was evaluated by determining the recovery ratio of OTC (recovery ratio = (detected concentration − background content)/added concentration). In brief, a series of known quantities of OTC standard was added to milk samples. The milk samples were pretreated by centrifugation separation (10 °C, 3500 rpm) for 10 min. Next, the supernatant was collected and diluted with PBS buffer proportionately (1 : 10 v/v). Finally, the OTC content of the resulting solution was measured with the developed aptasensor by the above-mentioned procedure. Furthermore, a commercially available ELISA method was also applied to detect OTC in the same milk samples.

3 Results and discussion

3.1 Detection principle

The luminescence bioassay platform for the detection of OTC based on upconversion and magnetic nanoparticles is illustrated in Fig. 1. Specifically, amino-modified MNPs were conjugated with an amino-modified aptamer *via* the classical glutaraldehyde method[35] to form the capture probes (aptamer-MNPs) and amino-modified $NaYF_4$:Yb, Er UCNPs were conjugated with amino-modified cDNA to form the signal probes (cDNA-UCNPs). Then the probes were hybridized to form MNPs-UCNPs signal probes.

After magnetic separation by an external magnet, the intensity of the emission peak at 544 nm was at a maximum in the absence of OTC, because of the abundance of the MNPs-UCNPs signal probes. Subsequently, OTC was added to the system and the aptamer preferentially bound to OTC, causing the dissociation of some cDNA, thereby liberating some cDNA-UCNPs. Finally, the intensity of the emission peak at 544 nm decreased as a result of the reduced concentration of MNPs-UCNPs signal probes.

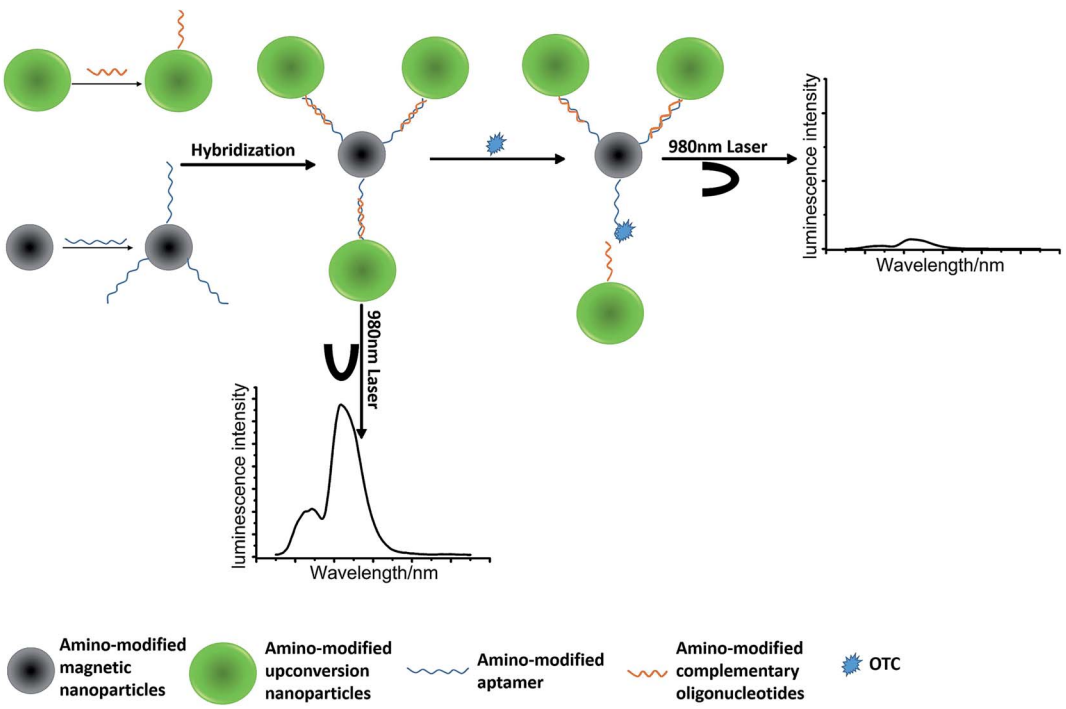

Fig. 1 Schematic illustration of the highly sensitive aptasensor for oxytetracycline based on upconversion and magnetic nanoparticles.

3.2 Design of complementary DNA sequences

In this study, we experimented with a sequence of the partially complementary strand of the aptamer, 5′-NH_2-CGGATCCACA-CAACA-3′. The basic principle of the cDNA design was that aptamers could adopt a defined conformation when binding to the targets and were also able to hybridize to the cDNA to form a duplex structure.[36,37] When designing the oligonucleotide strand of cDNA, proper care was taken to avoid excessive binding strength with the aptamer. When the targets and the complementary oligonucleotides were introduced, the aptamers preferentially bound to the targets, resulting in specific recognition of the targets.[38,39]

3.3 Preparation and characterization of UCNPs

The UCNPs were synthesized *via* a solvothermal method using chlorides. Transmission electron microscopy (TEM) images of the nanocrystals in Fig. 2a and b show the size and morphology of oleic acid-capped UCNPs. The NPs were then coated by the microemulsion method and characterized by TEM at the same time.

In this work, uniform $NaYF_4$ nanospheres with strong upconversion luminescence were produced, with a uniform silica coating on their surface. The microemulsion method has been one of the most commonly used methods for coating silica on nanocrystals. However, it is quite challenging to coat individual nanoparticles that have very thin shells. Thus, we have optimized the microemulsion method by adding different proportions of UCNPs and TEOS, finally resulting in a thickness of the silica shell of approximately 2 nm (Fig. 2c and d). By shortening the reaction time and increasing the UCNPs concentration, it is possible to create somewhat thinner layers of silica. After silica coating, the nanocrystals were dispersible in water and demonstrated good chemical and photochemical stability. Fig. 3 shows the luminescence intensity is only slightly reduced with the thin silica shell on the surface.

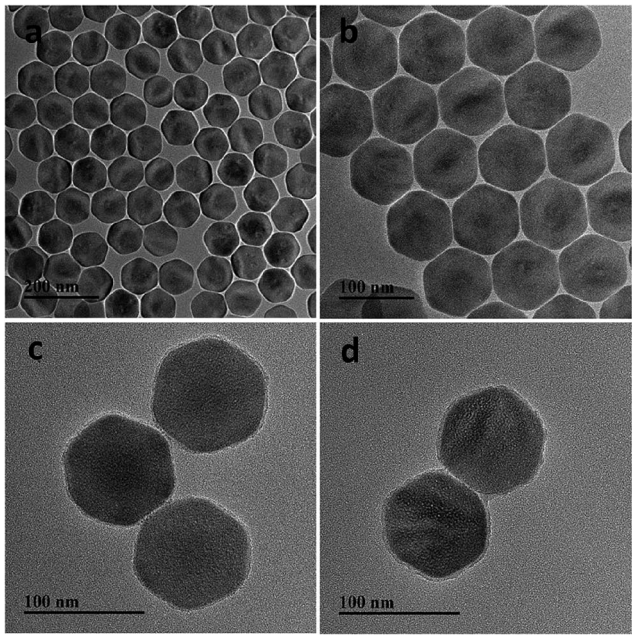

Fig. 2 TEM images of $NaY_{0.78}F_4$:$Yb_{0.20}$, $Er_{0.02}$ UCNPs before coating with silica (a and b) and after coating with silica (c and d).

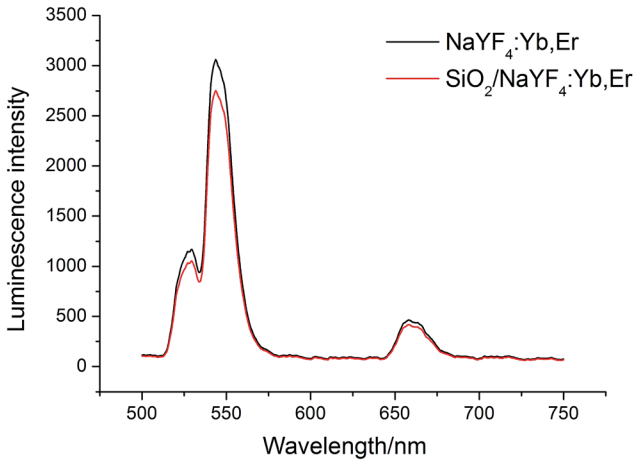

Fig. 3 Luminescence spectra of $NaYF_4$:Yb, Er nanospheres, with and without silica coating.

$NaYF_4$:Yb, Er nanocrystals have been shown to be the best NIR-to-visible upconversion luminescence materials and hexagonal-phase nanocrystals have higher upconversion efficiency than cubic-phase nanocrystals.[32] Fig. 4 gives the XRD patterns of $NaYF_4$:Yb, Er UCNPs, revealing the prepared UCNPs are purely hexagonal-phase (JCPDS no. 16-0334).

In addition to fabricating thin and uniform silica shells, the UCNPs were further functionalized with APTES to form an amino-terminated surface. The functional groups on the surfaces of the amino-modified $NaYF_4$:Yb, Er UCNPs are identified by FT-IR spectra in Fig. 5. The wide absorption peak at 3412 cm^{-1} in Fig. 5a is the stretching vibration of a hydroxyl group. The two peaks found at 1560 and 1458 cm^{-1} correspond to the asymmetric and symmetric stretching vibrations of a carboxylic group (COO^-). In addition, the bands at 2921 and 2853 cm^{-1} are assigned to the asymmetric and symmetric

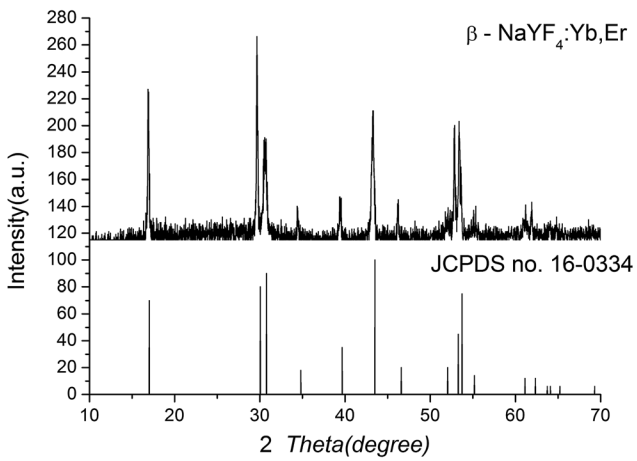

Fig. 4 XRD patterns of $NaYF_4$:Yb, Er UCNPs synthesized *via* method 1 (a) and method 2 (b).

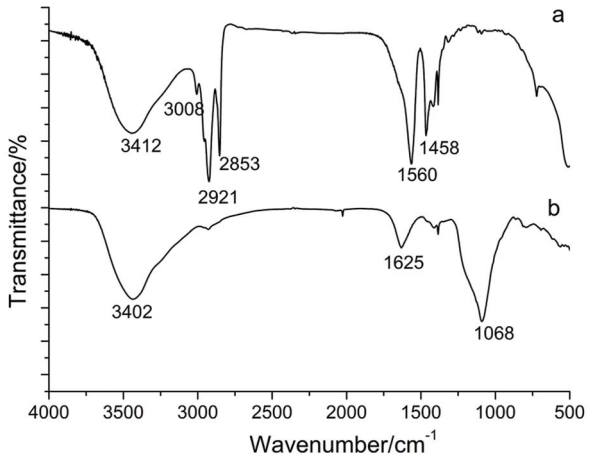

Fig. 5 FTIR spectra of UCNPs without silica shells (a) and with silica shells (b).

stretching vibrations of a methylene group, respectively, caused by the long-chain alkyl from oleic acid molecules. These results confirmed the UCNPs before modification were coated by oleic acid molecules. In contrast, the peaks mentioned above disappear altogether in Fig. 5b, and characteristic peaks corresponding to amino groups appear instead. The hydroxyl stretching vibration band of a silanol group (Si–OH) appears in the region of approximately 3402 cm^{-1}, and the band at 1068 cm^{-1} is attributed to the stretching vibration of a Si–O bond. The peak at 1625 cm^{-1} is the stretching and bending vibration bands of an amino group, indicating that the silica-coated UCNPs have been successfully functionalized with amino groups.

3.4 Preparation and characterization of MNPs

The amino-modified Fe_3O_4 MNPs used here were prepared by a one-pot synthesis. TEM (Fig. 6a) and FT-IR (Fig. 6b) were used to characterize the synthesized MNPs. It can be observed that the MNPs have an average size of approximately 25 nm. FT-IR spectroscopy shows a strong IR band at 583 cm^{-1}, which is characteristic of Fe–O vibrations. The transmissions at approximately 1632, 1396, and 1054 cm^{-1} from the amino-modified nanoparticles matched well with those from free 1,6-hexanediamine, indicating the existence of free $-NH_2$ groups on the amino-modified nanomaterials. The results from FT-IR revealed that the MNPs have been functionalized with amino groups in the synthetic process.

3.5 Characterization of amino-modified nanoparticles conjugated with amino-modified oligonucleotides

We applied UV-vis spectrophotometry to confirm the successful coupling of amino-modified oligonucleotides to amino-modified nanoparticles. As shown in Fig. 7, strong absorbance of the oligonucleotides can be seen at 260 nm, before conjugation to the nanoparticles. After incubation of the amino-modified nanoparticles and amino-modified oligonucleotides, the supernatant was collected by magnetic separation and centrifugation. The absorbance of the supernatant liquor was weaker at 260 nm, with a decrease in peak intensity, since part of the oligonucleotides had been combined with the amino-modified nanoparticles.

We further determined the number of oligonucleotides conjugated to nanoparticles by using a One Drop OD-1000 spectrophotometer. Initially, the concentration of the aptamer was 179 ng μL^{-1}. The concentration of the aptamer in the supernatant liquor collected after incubating with the MNPs (2 mg mL^{-1}) decreased to 35 ng μL^{-1}, indicating the conjugation yield between aptamer and MNPs was 77 000 ng mg^{-1}. Subsequently, the concentration of cDNA decreased from 104 ng μL^{-1} to 6 ng μL^{-1}, indicating the conjugation yield between cDNA and UCNPs was 49 000 ng mg^{-1}.

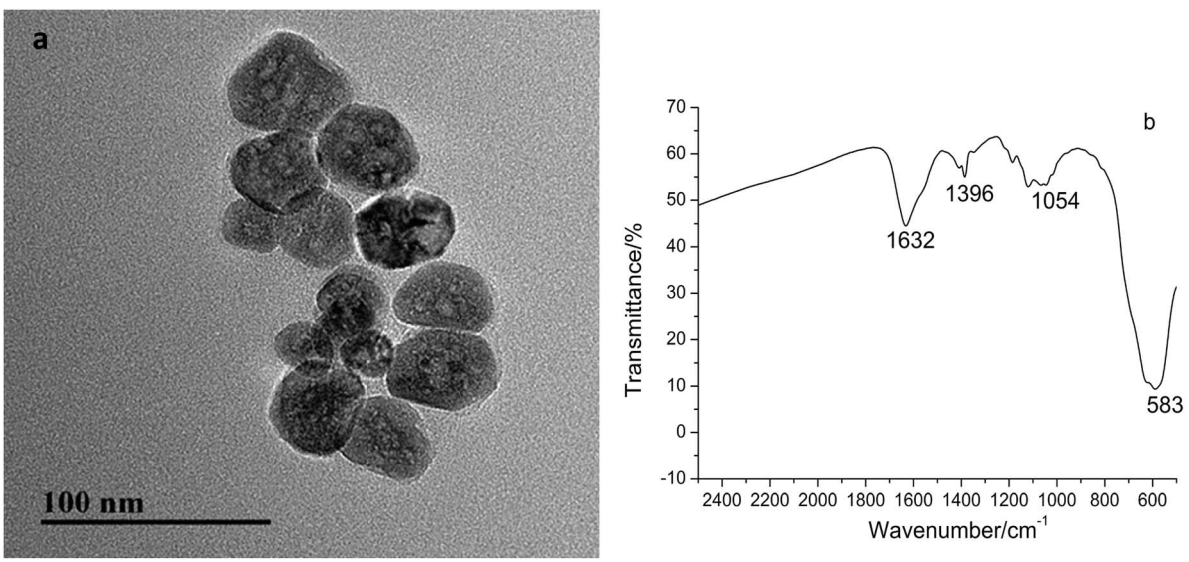

Fig. 6 TEM image (a) and FTIR spectrum (b) of the amino-modified Fe_3O_4 nanoparticles.

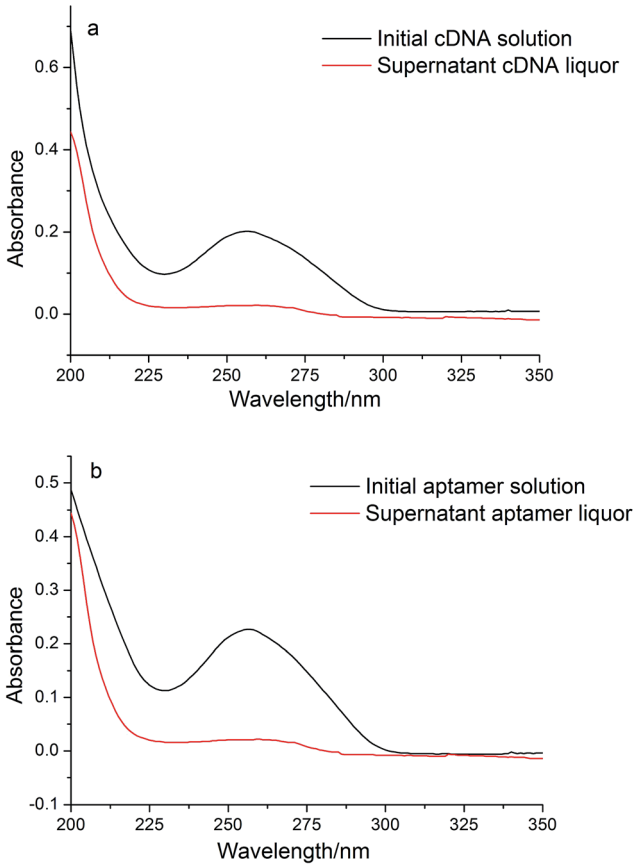

Fig. 7 UV-vis absorption spectra of cDNA solution (a) and aptamer solution (b) before and after conjugating with amino-modified nanoparticles (2 mg mL^{-1}).

3.6 Optimizing the dosage of probes

To identify the optimal dosages of cDNA-UCNPs and aptamer-MNPs, a comparative study was performed to determine the maximum background luminescence of UCNPs-MNPs probes. A total of 100 μL aptamer-MNPs and various volumes of cDNA-UCNPs solution were hybridized together. As shown in Fig. 8, the luminescence intensity increased with an increasing dose of cDNA-UCNPs solution, and the luminescence intensity reached a maximum with the addition of 800 μL cDNA-UCNPs solution. Initially, only a small quantity of UCNPs-MNPs was fabricated, as the low concentration of cDNA-UCNPs led to a large number of Apt-MNPs not having any cDNA-UCNPs to bind. When the concentration of cDNA-UCNPs and the concentration of Apt-MNPs were matched, the luminescence intensity reached a maximum. However, if the quantity of cDNA-UCNPs was in excess, the luminescence intensity of the UCNPs-MNPs decreased, because the cDNA-UCNPs were unable to combine with more aptamer-MNPs. The MNPs-UCNPs obtained at the optimal dosages formed a relatively stable suspension in a buffer, as shown in Fig. 9a. Fig. 9b shows the MNPs-UCNPs suspension emits green luminescence when excited by a 980 nm excitation laser.

Furthermore, we measured the luminescence intensity of the cDNA-UCNPs to determine the conjugation yield between Apt-MNPs and cDNA-UCNPs. The black line in Fig. 10 is the luminescence spectrum of the 800 μL cDNA-UCNPs solution before hybridizing with 100 μL Apt-MNPs. After hybridization of Apt-MNPs and cDNA-UCNPs, the supernatant was collected by magnetic separation and its luminescence was measured with a 980 nm excitation laser. As shown in Fig. 10, the intensity of the emission peak at 544 nm was reduced by about 41%, since part of the cDNA-UCNPs had been combined with amino-modified nanoparticles.

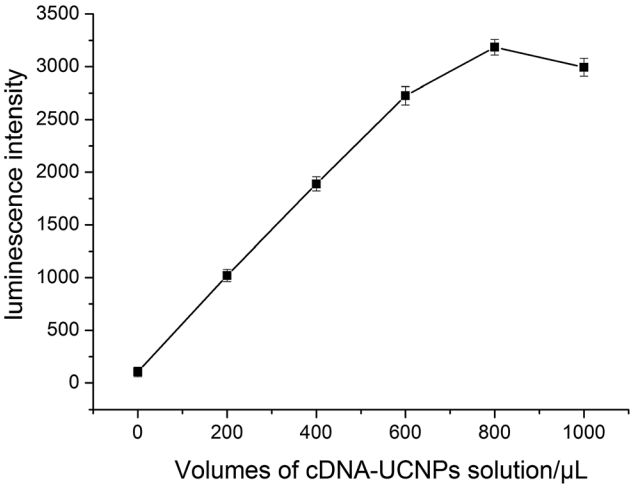

Fig. 8 Luminescence intensity of various volumes of cDNA-UCNPs (2 mg mL^{-1}) incubated with 100 μL aptamer-MNPs (2 mg mL^{-1}).

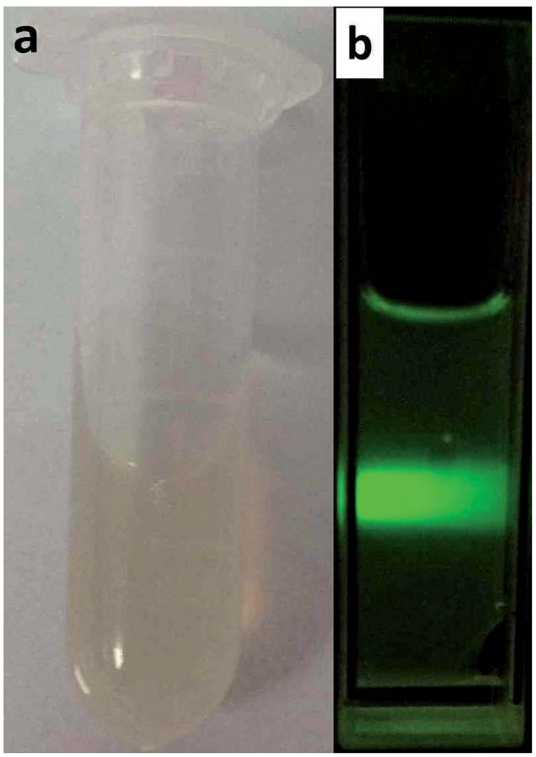

Fig. 9 Photographs of a MNPs-UCNPs suspension (a) and the luminescence of the suspension when excited by a 980 nm excitation laser (b).

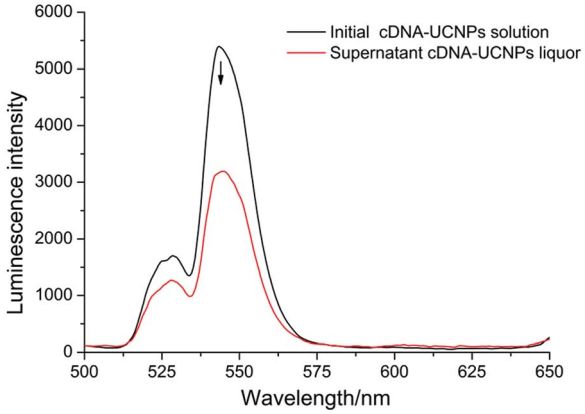

Fig. 10 Luminescence spectra of cDNA-UCNPs nanospheres (2 mg mL^{-1}) before and after hybridizing with 100 μL Apt-MNPs (2 mg mL^{-1}).

3.7 Optimizing the washing time

After a complete reaction between OTC and UCNPs-MNPs, the cDNA-UCNPs dissociated from UCNPs-MNPs should be washed thoroughly to prevent interference. Therefore, we optimized the washing time to give the best effect when washing. The UCNPs-MNPs probes were exposed to OTC (10 ng mL^{-1}) and buffer only, without OTC, respectively. The remaining UCNPs-MNPs were then separated by an external magnetic field and washed three times and the luminescence intensity was measured with a 980 nm excitation laser. The results are shown in Fig. 11. The luminescence intensity decreased with each increase in washing time and remained constant when the washing time was 15 s.

3.8 Determination of OTC

In this experiment, the luminescence intensity was at a maximum before the OTC was present. When the target molecule was introduced, the luminescence intensity decreased gradually as the aptamers preferentially bound to OTC and caused the dissociation of some cDNA-UCNPs from UCNPs-MNPs. Various intensities of the luminescence spectra obtained in the presence of different concentrations of OTC are shown in Fig. 12a. Fig. 12b shows the linear relationship between the intensity of the upconversion luminescence and the concentration of OTC. The LOD of the aptasensor for OTC is as low as 0.036 ng mL^{-1} (calculated by the function $3s/S$, where s is the standard deviation of the blank solution and S is the slope of

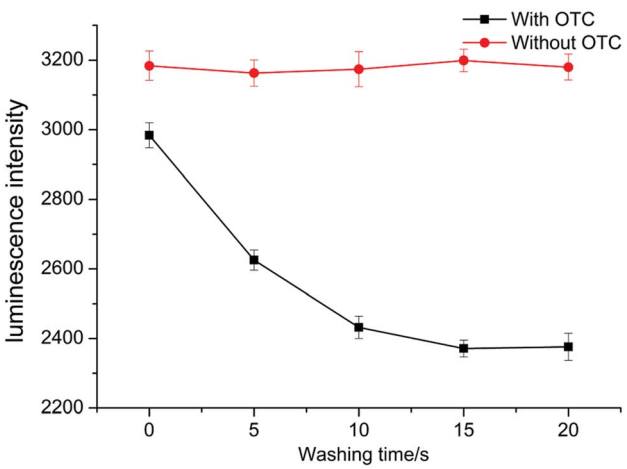

Fig. 11 Luminescence intensity for various washing times with OTC (10 ng mL^{-1}) and without OTC.

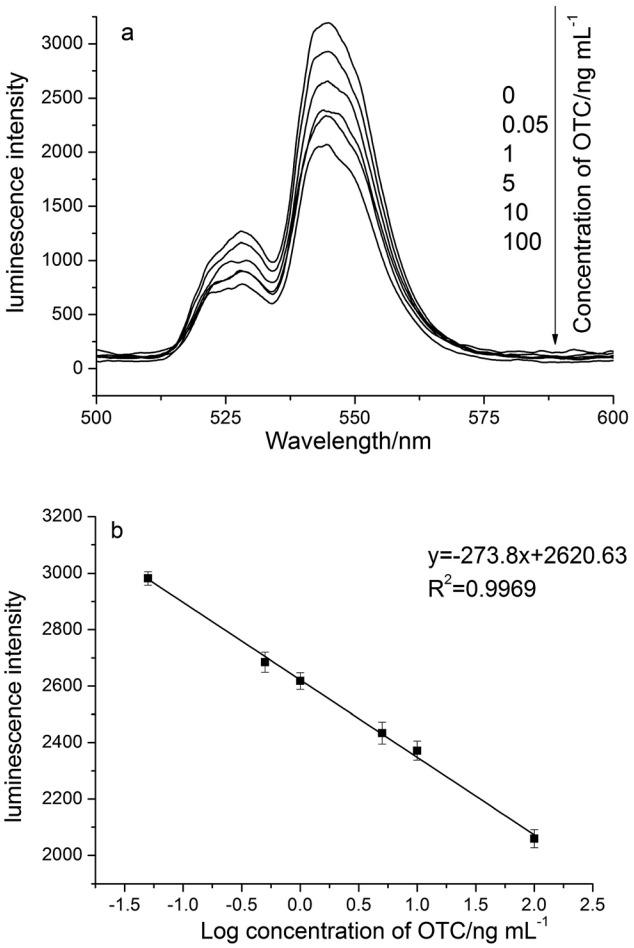

Fig. 12 Typical recording output for the detection of different concentrations of OTC (a); standard curve of the related upconversion luminescence intensity *versus* the log of the concentration of OTC (b).

Table 1 Reported detection methods for OTC and their limits of detection

Method	LOD	Reference
UHPLC method	0.2/0.003 ng mL^{-1}	19
Method based on indirect competitive ELAA	12.3 ng mL^{-1}	20
ELISA	7.01 ng mL^{-1}	21
Electrochemical determination	0.1 μM	24
Electrochemical biosensor	9.8 ng mL^{-1}	27
AuNP-based colorimetric assay	0.1 nM	29
Cantilever array sensors	0.2 nM	35
Fluorescent assay	10 nM	36

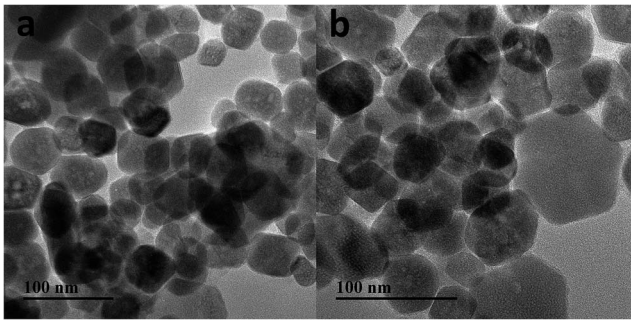

Fig. 13 TEM images of MNPs-UCNPs before (a) and after (b) treatment with the target.

the linear relationship). The precision, expressed by the relative standard deviation (RSD) of OTC detection, is 3.71% (10 ng mL^{-1}, $n = 10$). Table 1 presents some of the latest detection methods reported in recent years for OTC, which suggest that the proposed method has more sensitivity than most of those previously described.

Furthermore, we applied TEM to observe the morphology of MNPs-UCNPs before and after treatment with the target. Fig. 13a shows the morphology of MNPs-UCNPs before treatment with the target. After OTC was added to the system, the aptamer preferentially bound to OTC causing the dissociation of some cDNA, thereby liberating some cDNA-UCNPs. Fig. 13b shows the morphology of MNPs-UCNPs after treatment with the target.

3.9 Specificity

Three structurally similar tetracycline derivatives, including OTC, DOX, and TET, were used to confirm the good selectivity of this method. The aptasensor was exposed to these derivatives at the same concentration (10 ng mL^{-1}). The results are shown in Fig. 14. OTC caused a dramatic luminescence change, as was expected, while the others failed. The good specificity of this method was attributed to the inherent specificity of the aptamer toward OTC.

3.10 Analytical application

The accuracy of OTC detection in food samples was evaluated by determining the recovery ratio of OTC by adding a series of known quantities of OTC into milk samples. As shown in Table 2, the recovery ratios were between 98.60% and 119.00%, and there was no significant difference ($p < 0.0001$) between the results obtained by the aptasensor and an ELISA method in Fig. 15, indicating the proposed aptamer-based bioassay can be applied for OTC detection in food samples.

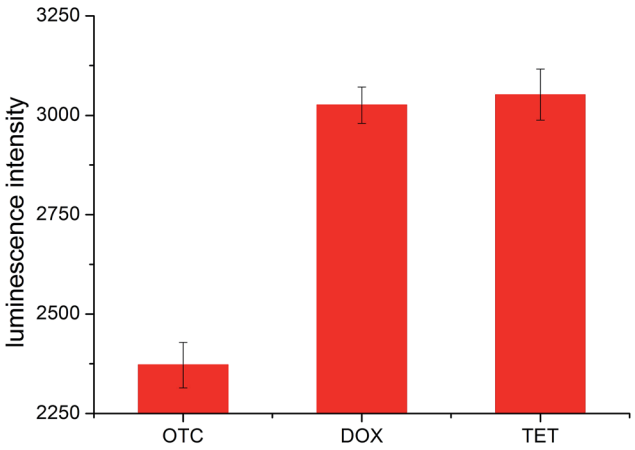

Fig. 14 Differential luminescence response of the aptasensor at 544 nm to OTC, DOX, and TET at the same concentration (10 ng mL^{-1}).

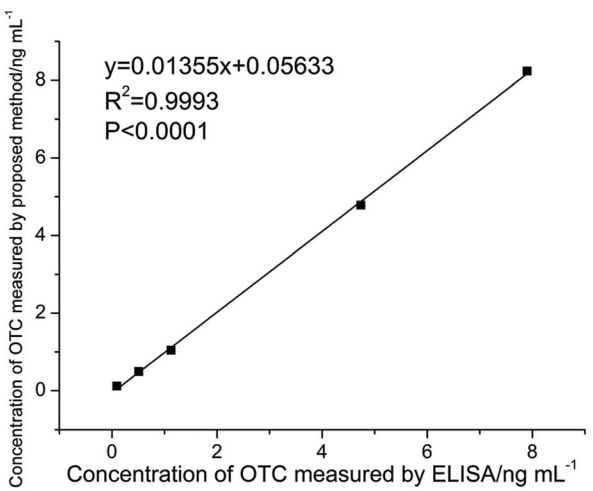

Fig. 15 Relationship between the proposed method and ELISA method for OTC detection.

Table 2 Recovery ratio results for added standard OTC from milk samples obtained by the developed method

Sample	Background content (ng mL^{-1})	Added concentration (ng mL^{-1})	Detected concentration (ng mL^{-1})		Recovery ratio (%)
			ELISA	Aptasensor	
1	0	0.1	0.093	0.119	119.00
2	0	0.5	0.512	0.493	98.60
3	0	1	1.127	1.042	104.20
4	0	5	4.738	4.782	95.64
5	0	8	7.901	8.232	102.75

4 Conclusions

In this study, a highly sensitive aptasensor for the rapid and specific detection of OTC, based on upconversion and magnetic nanoparticles, was successfully developed and evaluated. Typically, the use of UCNPs entirely avoided auto-luminescence originating from biomolecules possibly contained in the solution, as the UCNPs were excited by an infrared 980 nm laser. Furthermore, magnetic separation simplified the experimental processes as the magnetic nanoparticles can concentrate and separate targets from a food solution easily and rapidly. Lastly, the aptamers were stable compared to traditional antibodies and highly specific to the target OTC. In summary, the aptasensor offers a new approach of high convenience, sensitivity, specificity, and stability to detecting OTC in food samples.

Acknowledgements

This work was partly supported by the National S&T Support Program of China (2012BAK08B01), NSFC (21375049), S&T Supporting Project of Jiangsu Province (BE2011621) and JUSRP51309A.

References

1 C. Liu, H. Yi and M. Gao, *Adv. Mater.*, 2014, **26**, 6922–6932.
2 P. Wang, P. Joshi, A. Alazemi and P. Zhang, *Biosens. Bioelectron.*, 2014, **62**, 120–126.
3 A. Xia, X. Zhang, J. Zhang, Y. Deng, Q. Chen, S. Wu, X. Huang and J. Shen, *Biomaterials*, 2014, **35**, 9167–9176.
4 Z. Gu, L. Yan, G. Tian, S. Li, Z. Chai and Y. Zhao, *Adv. Mater.*, 2013, **25**, 3758–3779.
5 Q. Zhan, S. He, J. Qian, H. Cheng and F. Cai, *Theranostics*, 2013, **3**, 306–316.
6 Y. Zhai, C. Zhu, J. Ren, E. Wang and S. Dong, *Chem. Commun.*, 2013, **49**, 2400–2402.
7 F. Lin, B. Yin, C. li, J. Deng, X. Fan, Y. Yi, C. Liu, H. Li, Y. Zhang and S. Yao, *Anal. Methods*, 2013, **5**, 699.
8 X. Li, Z. Li, W. Gan, T. Wang, S. Zhao, Y. Lu, J. Cheng and G. Huang, *Analyst*, 2013, **138**, 3711–3718.
9 S. Hao, G. Chen and C. Yang, *Theranostics*, 2013, **3**, 331–345.
10 L. Cheng, C. Wang, X. Ma, Q. Wang, Y. Cheng, H. Wang, Y. Li and L. Zhuang, *Adv. Funct. Mater.*, 2013, **23**, 272–280.
11 S. Wu, N. Duan, C. Zhu, X. Ma, M. Wang and Z. Wang, *Biosens. Bioelectron.*, 2011, **30**, 35–42.
12 S. Wu, N. Duan, Z. Wang and H. Wang, *Analyst*, 2011, **136**, 2306–2314.
13 Z. Huang, S. Wu, N. Duan, D. Hua, Y. Hu and Z. Wang, *J. Pharm. Biomed. Anal.*, 2012, **66**, 225–231.
14 S. Graslund and B.-E. Bengtsson, *Sci. Total Environ.*, 2001, **280**, 93–131.
15 A. Stolker and U. Brinkman, *J. Chromatogr. A*, 2005, **1067**, 15–53.
16 S. A. de Albuquerque Fernandes, A. P. Magnavita, S. P. Ferrao, S. A. Gualberto, A. S. Faleiro, A. J. Figueiredo and S. V. Matarazzo, *Environ. Sci. Pollut. Res.*, 2014, **21**, 3427–3434.
17 Á. Tölgyesi, L. Tölgyesi, K. Békési, V. K. Sharma and J. Fekete, *Meat Sci.*, 2014, **96**, 1332–1339.
18 K. Škrášková, L. H. Santos, D. Šatínsk, A. Pena, M. C. Montenegro, P. Solich and N. Nováková, *J. Chromatogr. B: Anal. Technol. Biomed. Life Sci.*, 2013, **927**, 201–208.
19 C.-H. Kim, L.-P. Lee, J.-R. Min, M.-W. Lim and S.-H. Jeong, *Biosens. Bioelectron.*, 2014, **51**, 426–430.
20 T. Wongtangprasert, W. Natakuathung, U. Pimpitak, A. Buakeaw, T. Palaga, K. Komolpis and N. Khongchareonporn, *J. Zhejiang Univ., Sci., B*, 2014, **15**, 165–172.
21 N. Ajami, N. Bahrami Panah and I. Danaee, *Iran. Polym. J.*, 2013, **23**, 121–126.
22 W. Yun, H. Li, S. Chen, D. Tu, W. Xie and Y. Huang, *Eur. Food Res. Technol.*, 2014, **238**, 989–995.
23 X. Ma, W. Wang, X. Chen, Y. Xia, S. Wu, N. Duan and Z. Wang, *Eur. Food Res. Technol.*, 2014, **238**, 919–925.
24 D. Zheng, X. Zhu, X. Zhu, B. Bo, Y. Yin and G. Li, *Analyst*, 2013, **138**, 1886–1890.
25 J. H. Niazi, S. J. Lee, Y. S. Kim and M. B. Gu, *Bioorg. Med. Chem.*, 2008, **16**, 1254–1261.
26 Y. S. Kwon, N. H. Ahmad Raston and M. B. Gu, *Chem. Commun.*, 2014, **50**, 40–42.
27 Y. S. Kim, J. H. Niazi and M. B. Gu, *Anal. Chim. Acta*, 2009, **634**, 250–254.
28 Y. S. Kim, J. H. Kim, I. A. Kim, S. J. Lee, J. Jurng and M. B. Gu, *Biosens. Bioelectron.*, 2010, **26**, 1644–1649.
29 K. Kim, M. B. Gu, D. H. Kang, J. W. Park, I. H. Song, H. S. Jung and K. Suh, *Electrophoresis*, 2010, **31**, 3115–3120.
30 H. Hou, X. Bai, C. Xing, N. Gu, B. Zhang and J. Tang, *Anal. Chem.*, 2013, **85**, 2010–2014.
31 H. Zhao, S. Gao, M. Liu, Y. Chang, X. Fan and X. Quan, *Microchim. Acta*, 2013, **180**, 829–835.
32 Z. Li and Y. Zhang, *Nanotechnology*, 2008, **19**, 345606.
33 Z. Li, Y. Zhang and S. Jiang, *Adv. Mater.*, 2008, **20**, 4765–4769.
34 L. Wang, J. Bao, L. Wang, F. Zhang and Y. Li, *Chem.–Eur. J.*, 2006, **12**, 6341–6347.
35 X. Hun and Z. Zhang, *Biosens. Bioelectron.*, 2007, **22**, 2743–2748.
36 N. Hamaguchi, A. Ellington and M. Stanton, *Anal. Biochem.*, 2001, **294**, 126–131.
37 R. Nutiu and Y. Li, *J. Am. Chem. Soc.*, 2003, **125**, 4771–4778.
38 W. U. Dittmer, A. Reuter and F. C. Simmel, *Angew. Chem., Int. Ed.*, 2004, **43**, 3550–3553.
39 Y. Xiao, B. D. Piorek, K. W. Plaxco and A. J. Heeger, *J. Am. Chem. Soc.*, 2005, **127**, 17990–17991.